doi: 10.34248/bsengineering.1790069



Research Article

Volume 9 - Issue 1: XX-XX / January 2026

SPECTROSCOPIC APPROACHES TO CULTURAL HERITAGE OBJECTS: A MORIAGE-DECORATED JAPANESE DRAGONWARE PLATE

Duygu TAKANOGLU BULUT1*

¹Pamukkale University, Application of Advanced Technology and Research Center (ILTAM), 20160, Denizli, Türkiye

Abstract: In this study, the material composition and coloration strategies of the three moriage enamel colors (white, black, and orange) on a Japanese Dragonware plate were elucidated through a multi-technique approach. X-ray fluorescence (XRF) was employed to determine the bulk-averaged chemistry. Energy-dispersive spectroscopy (EDS) point analysis was performed to assess microscale compositions and elemental distributions. Fourier-transform infrared spectroscopy (FT-IR) was used to evaluate the polymerization/depolymerization behavior of the silicate glass network, and Raman spectroscopy was applied to fingerprint the pigment phases. It was demonstrated that the enamels were produced with color-specific formulations. In DW-W (white), a Pb and alkali-rich, low-melting, and fluid Pb-alkali silicate binder was identified. In DW-B (black), a more depolymerized network was identified, attributed to the dilution of the glass phase by the pigment, and this assessment was supported by the presence of a carbon-based pigment, as verified by Raman and EDS results. In DW-0 (orange), an Al-rich feldspathic framework together with hematite (α-Fe₂O₃), signatures were observed. Differences in the position and bandwidth of the ~900-1100 cm⁻¹ asymmetric Si-O band in FT-IR, together with the D1/D2 ring modes in Raman, were found to indicate different degrees of network polymerization among the colors. Across the Raman and FT-IR analyses, the absence of crystalline quartz fingerprints together with the presence of broad glass bands was taken to confirm that the enamels were embedded within an amorphous glass matrix. These results were considered to evidence an overglaze technology involving low-temperature, multi-step firing and color-specific recipes. The findings are proposed as a scalable analytical template for classification and conservation strategies in multilayer decorative systems such as moriage-enameled Dragonware.

Keywords: Overglaze enamel, XRF analysis, FT-IR analysis, Raman analysis, Cultural heritage objects

*Corresponding author: Pamukkale University, Application of Advanced Technology and Research Center (ILTAM), 20160, Denizli, Türkiye

E mail: dbulut@pau.edu.tr (D. TAKANOGLU BULUT)

Cite as: Takanoglu Bulut, D. (2026). Spectroscopic approaches to cultural heritage objects: A Moriage-decorated Japanese Dragonware plate. Black Sea Journal of Engineering and Science, 9(1), xx-xx.

1. Introduction

The analysis of cultural heritage materials elucidates the culture, trade, and technology of their periods, providing valuable insights into the past (Veeramuthu et al., 2014). Within this framework, ceramic and porcelain materials have become a primary focus of researchers (Weber et al., 1990; Mommsen et al., 1992; Veeramuthu et al., 2014). Regarding ceramic and porcelain cultural heritage objects, determining the material composition, assessing authenticity, elucidating manufacturing technologies, and defining conservation strategies are regarded as fundamental steps (Giannossa et al., 2021). Within the field of ceramic and porcelain heritage studies, Japanese ceramics have been recognized for their exemplary craftsmanship, technologically advanced production practices, and a distinctive vocabulary of motifs. In this methodological framework, an appropriate basis is provided for evaluating the cultural and historical context of Dragonware, which is recognized as an export-

oriented typology in the history of Japanese ceramics. Dragonware has been characterized as an export category that came to prominence within the exportoriented production wave of the Meiji (1868-1912), Taishō (1912-1926), and early Shōwa (1926-1945) periods; during this time, with the opening of foreign trade, production and distribution networks directed toward Western markets were rapidly expanded (Coman, 2021). In East Asian iconography, the dragon motif has long been associated with power, protection, and prosperity, and in the late nineteenth and early twentieth centuries, it was frequently deployed in dramatic compositions adapted to Western tastes for export (Willmann, 2011). Against this backdrop, raised enamel trails executed by the moriage (icchin/piping) technique, in conjunction with low-temperature overglaze applications and high-contrast color palettes (e.g., white-black-orange accents), were established as distinguishing manufacturing and aesthetic strategies of

the repertoire (Anonymous, 2024). The designation 'Dragonware' is encountered in productions initiated during the Meiji period and continuing into the first half of the twentieth century; the objects were marketed in series across different quality and price segments, and in specific workshops and factories, semi-serial decoration routines were combined with handicraft (Nilsson, 2023). The export orientation of production and the prevalence of overglaze enameling reveal the intersection of the period's market orientation, manufacturing technology, and iconography; a comparable trajectory is also observed in other export groups, such as Satsuma, characterized by polychrome enamel and gilt repertoires adapted to Western tastes. Situated within this exportoriented visual economy, Dragonware objects also present analytical challenges arising from their multilayered structures, aging processes, and subsequent additions. Therefore, the development of an interdisciplinary strategy grounded in non-destructive techniques and micro-sampling is of particular importance (Boon et al., 2006; Prati et al., 2010; Papliaka et al., 2015; Pięta et al., 2019). A large proportion of archaeological questions can be addressed through the integrated application of analytical methods that provide compositional and structural information on the bulk or surface of the sample (Giannossa et al., 2021). This multifaceted analytical requirement underscores the integrated application of spectroscopic techniques that differ in the physical quantities they measure as well as in their spatial resolutions and effective probing depths. In addition, similarities and differences in the raw material compositions of examined samples can be revealed by spectroscopic techniques (Öz et al., 2019). In cultural heritage research, the integrated reporting of results obtained using spectroscopic and microscopic techniques, such as X-ray fluorescence (XRF), scanning electron microscopy coupled with energy-dispersive Xray spectroscopy (SEM-EDS), Fourier-transform infrared spectroscopy (FT-IR), and Raman spectroscopy, are reliable essential for the identification characterization of the studied objects (Pieta, et al., 2019).

In the context of elemental analysis, XRF, in which the energies and intensities of emitted characteristic X-rays are measured, is widely recognized as a prominent physical technique for determining the major, minor, and trace elemental compositions of cultural heritage objects, such as ceramic and porcelain items (Szökefalvi-Nagy et al., 2004; Hunt and Speakman, 2015; Hunt, 2017). Understanding the chemical composition (SiO2, Al2O3, K2O, CaO, Fe2O3, etc.) of ceramic and porcelain materials is critical for classifying ceramic body types, identifying glaze types, inferring production recipes and raw materials, and potentially providing a basis for provenance studies (Bezur and Casadio, 2013).

Integrated into a scanning electron microscope, energy-dispersive X-ray spectroscopy (EDS) is based on the measurement of the energy spectrum of characteristic X-

rays generated as the inner shells of specimen atoms are ionized by a focused electron beam (Scimeca et al., 2018). In porcelain and glaze studies, local elemental distributions can be resolved by EDS, enabling the discrimination between the glassy matrix and crystalline pigment/opacifier grains and permitting inferences about formulation and firing conditions (Turco et al., 2017; Moropoulou et al., 2019). Whereas XRF analysis provides bulk or area-averaged composition, EDS analysis targets micrometer-scale heterogeneities and establishes correlations between morphology and chemistry. The combined use of the two techniques enhances the accuracy and interpretive power of the analyzed material's composition (Turco et al., 2017; Perna et al., 2024).

FT-IR spectroscopy is defined as a technique directly sensitive to the molecular vibrations, and it is widely applied in cultural heritage studies to characterize organic binders, varnishes, and adhesives, as well as inorganic pigments, corrosion products, salts, and glass/glaze phases (Prati et al., 2016). Infrared radiation interacts with molecules, causing the characteristic vibration of chemical bonds, and the resulting absorption spectrum allows for the identification of molecules (Ricci, 2016). FT-IR analysis is widely endorsed in conservation science as a non-destructive or micro-destructive approach, and reliable material identification can be achieved even in complex and aged matrices (Liu and Kazarian, 2022). In archaeometric studies of ceramics, changes in position, intensity, and shape of IR bands (Si-O, Al-O-Si, etc.) are employed to elucidate body technology and thermal history (Ricci, 2016).

Owing to its high spatial resolution, minimal sample preparation requirements, and most importantly, its non-destructive nature, Raman spectroscopy is regarded as an essential analytical technique for analyzing cultural heritage objects and complex materials such as ceramics and porcelain (Bell et al., 1997; Ravindran et al., 2011; Pieta et al., 2014). Molecular and crystal-lattice vibrations are examined by Raman spectroscopy; therefore, the technique is highly sensitive to composition, bonding, chemical environment, phase, and crystal structure (Smith and Clarke, 2004). Unlike elemental analysis methods such as XRF and EDS, direct information on the molecular structure of the material is provided by Raman spectroscopy, enabling the precise identification of existing crystalline and amorphous phases (Smith and Clark, 2004). This capability is particularly advantageous in the analysis of historic glazes; the amorphous silicate network constituting the glass matrix can be characterized, and the types of micron-sized pigment particles (e.g., oxides, sulfates, or carbon-based pigments) responsible for color and opacity can be clearly distinguished (Colomban, 2004). Within this analytical framework, a color-resolved, multitechnique case study was conducted on a moriage decorated Dragonware porcelain plate, a representative example of a layered and heterogeneous structure. Bulk

composition was determined by X-ray fluorescence (XRF); micrometer-scale verification and distribution were assessed by scanning electron microscopy coupled with energy-dispersive X-ray spectroscopy (EDS); the chemistry of the glassy network was characterized by Fourier-transform infrared spectroscopy; pigment/mineral phases were identified by Raman spectroscopy, so that an integrated interpretation could be established. In this manner, differences in formulation among the colors and potential pigment strategies, together with degrees of glass network depolymerization/polymerization and the presence of carbon additives of potential conservation relevance, were targeted for elucidation.

2. Materials and Methods

2.1. Materials

The object examined in this study is a representative example of the 'Dragonware' porcelain plate category, produced in twentieth-century Japan and shown in Figure 1. The term 'Dragonware' is used to designate porcelain that were heavily exported from Japan to Western markets from the nineteenth to the midtwentieth century, whose principal decorative element is a prominent dragon figure (Nilsson, 2023). The embossed dragon figures, the most distinctive feature of these wares, were produced by a technique known in Japanese ceramic art as 'Moriage'.



Figure 1. Moriage decorated Japanese Dragonware plate.

Moriage is defined as a technique in which threedimensional relief decoration is produced on porcelain surfaces by piling up slip or enamel in string-like lines or droplets (Nilsson, 2023). In practice, fine-tipped icchin/itchin (piping) tools, bamboo tubes, or conical materials have typically been employed, and the method is also referred to as tubelining/slip trailing (Anonymous, 2024; Anonymous, 2025). Moriage produces raised, 'cake frosting' in appearance and is reported as a prevalent decorative feature on Japanese export ceramics from the late nineteenth to the midtwentieth century (Nilsson, 2023). Dragonware pieces were produced in a wide variety of forms, including tea sets, plates, vases, and decorative objects, for Western markets, and have been highly prized by collectors (Nilsson, 2023).

The object examined in this study is a Dragonware plate with a shallow concave body and an approximate diameter of 22 cm. The plate is coated with a glossy glaze that carries a thin gilt band along the rim. The ground color exhibits a gradient effect, transitioning softly from pale yellowish-green at the center to light to medium green toward the rim, with occasional cool blue hues. The principal composition is formed by a dragon figure executed in the moriage technique, which encircles the surface clockwise. The moriage relief is of pronounced height, rises above the surface, and displays localized thickening. The dragon figure has been detailed with white, black, and orange moriage relief enamels. The white enamel is used predominantly on the body, while the black enamel emphasizes details such as scales, eyes, and claws. The orange enamel provides vivid contrast in selected areas surrounding the composition, serving as a decorative element.

Within the scope of this study, powder samples were collected from white, black, and orange regions of the moriage layers by micro-scraping and were labeled DW-W (white), DW-B (black), and DW-O (orange), respectively.

2.2. Methods

In this study, powder samples coded DW-W, DW-B, and DW-O were measured to obtain (i) bulk chemistry by XRF, (ii) micrometer-scale verification and elemental distribution by EDS, (iii) the vibrational signature of the glass network by FT-IR, and (iv) pigment/mineral fingerprints by Raman spectroscopy. The results were interpreted in an integrated, color-resolved manner.

To determine the chemical composition of different colored moriage layers, a Spectro XEPOS (PED-XRF, Germany) X-ray fluorescence spectrometer was employed. The XRF system is equipped with a 50 W Pd Xray tube, providing a spectral resolution of 160 eV. Measurements were performed on micro-scraped powder samples, and the elemental concentrations were reported as oxide equivalents. The microscopic chemical compositions and elemental distributions of the moriage reliefs were assessed by point analyses using energydispersive spectroscopy (EDS), integrated into a fieldemission scanning electron microscope (FE-SEM). The system was used a Zeiss Supra 40 VP (Germany), operated at an accelerating voltage of 20 kV and a working distance of 9.6 mm. The FT-IR spectra of the samples were recorded using a PerkinElmer Spectrum Two (USA) spectrometer over the 400-4000 cm⁻¹ midrange. The spectra were evaluated with respect to the amorphous glass matrix and to inorganic and organic

functional groups. The electronic and vibrational properties, together with symmetry information, were acquired using the BWTEK BWS465-785S i-Raman (USA) system. A 785 nm laser was employed, and the spectrometer range was set to 100-1600 cm⁻¹. Low laser power and appropriate integration times were selected to minimize photothermal effects.

Data obtained by all techniques were evaluated independently for each colored relief and were integrated into a comprehensive interpretation.

3. Results and Discussions

3.1. XRF Analyses

The bulk chemical compositions of moriage enamels were established by XRF measurements, thereby providing a chemical framework for the interpretation of phase-specific (FT-IR, Raman) and microanalytical (EDS) methods. Powder samples of different colors were analyzed under identical conditions. Thus, elemental variations among the colors were determined independently of surface effects. The weight percent chemical compositions of different-colored moriage enamels, determined by XRF, are given in Table 1.

Table 1. Elemental compositions of moriage enamels

Element	DW-W	DW-B	DW-0
Na ₂ O	4.359	2.479	5.009
MgO	0.017	0.063	0.084
Al_2O_3	14.121	10.017	16.872
SiO_2	50.532	52.783	57.917
P_2O_5	0.069	0.102	0.005
SO_3	1.044	0.203	0.298
K_2O	10.049	17.083	8.324
CaO	0.41	0.5	0.251
TiO_2	0.162	0.277	0.133
Fe_2O_3	0.547	0.731	0.959
Cr_2O_3	0.006	0.009	0.003
MnO	0.012	0.0167	0.007
PbO	17.774	14.515	9.496

Upon examination of the XRF results for DW-W (white), DW-B (black), and DW-O (orange) moriage enamels, systematic variations within the lead-alkali-silicate system were observed as a function of color. The highest PbO content (17.77 wt.%) was found in the DW-W, whereas SiO_2 and Al_2O_3 were present at moderate levels, and the alkali oxides were identified as network-modifying constituents (K_2O 10.05 wt.%, Na_2O 4.36 wt.%). This distribution is consistent with high lead overglaze enamel formulations typical of opaque/glossy relief decoration and has been reported for color-tuned Pb-silicate enamels in Qing-period and Japanese on-glaze (akea, moriage) applications (Colomban et al., 2022).

The preference for lead as a flux in enamels is commonly attributed to its ability to effectively depolymerize the silicate network, thereby providing fusibility and fluidity at low firing temperatures. In addition, the high polarizability of Pb^{2+} ions has been reported to lower the

bond-breaking energy of Si-O bridges and to reduce the viscosity of the glass network. As a result, the softening/melting temperature of the enamel layer is markedly depressed. This functional role has been clearly documented in studies of Chinese overglaze enamels and in the Japanese akae tradition (Qu et al., 2017; Inada et al., 2018; Colomban et al., 2022; Li et al., 2024).

The oxide composition of DW-B was found to be an alkali-oxide-rich composition ($K_2O = 17.08 \text{ wt.}\%$, $Na_2O =$ 2.48 wt.%, PbO = 14.52 wt.%, SiO₂ = 52.78 wt.%, and $Al_2O_3 = 10.02$ wt.%). This distribution indicated that the enamel's chemistry is characterized by an elevated potassium content. In silicate networks, alkali oxides are known to act as network-modifying constituents that generate non-bridging oxygens (NBOs), thereby lowering melt viscosity; consequently, the flow required for line/contour relief decoration is facilitated (Wu and Stebbins, 2009). In this parallel, recent classification studies have reported that overglaze enamels can be grouped as lead-rich, alkali-rich, or lead-modified alkali types, and that compositional differences can be reliably discriminated by Raman/XRF analysis (Jiusti et al., 2020; Colomban et al., 2024). Within this framework, the DW-B enamel was inferred to be consistent with an alkali-rich, Pb-modified profile.

Relative to the other colors, the DW-O (orange) was found to have the lowest PbO content (9.50 wt.%) and the highest SiO₂-Al₂O₃ pair (57.92 and 16.87 wt.%, respectively); the alkali oxides K2O and Na2O were present at 8.32 and 5.01 wt.%, respectively. This composition was interpreted as consistent with networkformer-rich (feldspathic) glass formulation (Shackelford and Doremus, 2008). In ceramic enamels, orange and red hues have been widely reported to be achieved through the incorporation of hematite (Fe₂O₃). Moreover, the intensity of the color has been shown to be governed not by the mass percentage of hematite employed but by its dispersion and particle size within the Pb and alkali silicate glass matrix, together with dissolutionreprecipitation dynamics (Hashimoto et al., 2016a; Hashimoto et al., 2016b). A Fe₂O₃ content of approximately 0.96 wt.% was measured in DW-0, which was interpreted to indicate that the color-bearing pigment was employed at a low yet functional loading and that the observed hue was likely attributable to hematite. The elevated Si-Al network and the relatively low Pb content of the DW-O were considered consistent with the presence of a pigment-bearing, more polymerized (feldspathic) matrix (Hashimoto et al. 2016b; Qu et al., 2017; Inada et al., 2018).

A progressive variation in the PbO/SiO $_2$ and K_2 O/SiO $_2$ ratios among differently colored moriage enamels was taken as evidence that layer formulations were optimized for their functions. Specifically, PbO/SiO $_2$ ratios of 0.352, 0.275, and 0.164 were measured for DW-W, DW-B, and DW-O, respectively. The corresponding K_2 O/SiO $_2$ ratios were 0.199, 0.324, and 0.144.

Accordingly, a Pb-rich composition was considered to have been employed in DW-W to promote opacity/gloss; an alkali-rich composition was supposed to have been used in DW-B to ensure fluid contour lines. A Si-Al network-rich (feldspathic) glass formulation was considered to have been employed in DW-O. These results are consistent with archaeometric literature, in which overglaze enamels are reported to be compositionally tuned across multiple firings and lead is preferred for its low-temperature fusibility and

processing advantages (Colomban et al., 2022b).

3.2. EDS Analysis

In this section, point analysis performed by energy dispersive spectroscopy (EDS) integrated with a field emission scanning electron microscope (FE-SEM) was presented, and these data were evaluated to clarify the microscale correlates of the compositional trends obtained by XRF. In Table 2, the EDS results were reported as weight percentages (wt.%) for DW-W, DW-B, and DW-O.

Table 2. EDS results of DW-W, DW-B, and DW-O

Moriage Enamel	0	Si	Pb	Al	K	Na	Fe	С
DW-W	33.52	34.03	15.66	7.12	9.24	0.43	-	-
DW-B	31.44	31.98	11.82	7.02	4.07	0.73	-	12.94
DW-O	39.29	32.14	10.58	9.38	6.02	0.93	1.66	-

As seen in Table 2, the three moriage enamels were formulated with distinct pigment strategies at the microscale. By the nature of the method, these data are considered representative of the local composition of the analyzed regions. Moreover, in heterogeneous systems such as enamels, the ability to provide phase-specific information is regarded as one of the principal advantages of EDS.

In DW-W, a composition of 15.66 wt.% Pb, 9.24 wt.% K, 34.03 wt.% Si and 7.12 wt.% Al was measured, and it was considered diagnostic of a low-melting, highly fluid leadalkali silicate matrix. Historically, the use of Pb-rich and Pb-alkali glass compositions in overglaze enamels is well-documented in classification studies and field practice (Colomban et al., 2018; Colomban et al., 2022b). In this context, the elevated Pb/Si (~0.46) and K/Si (~ 0.27) ratios were considered to indicate that PbO and K_2O served as network modifiers, thereby depolymerizing the silicate network and lowering the melting and viscosity thresholds. The fluxing role of lead and alkali oxides in low-temperature glaze and enamel technologies is clearly defined in the glass literature (Tite et al., 1998; Pradell and Molera, 2020).

In DW-B, a composition of 11.82 wt.% Pb, 4.07 wt.%K, 31.98 wt.% Si, 7.02 wt.% Al, 0.73 wt.% Na and a prominent 12.94 wt.% C was measured. It was considered indicative of a carbon-based pigment dispersed within the glass matrix. Historically, the presence of carbon in black contour/line areas of overglaze enamels is well documented (Colomban et al., 2018). In this layer, the lower flux ratios, Pb/Si~0.37 and K/Si~0.13, were considered to indicate a formulation with comparatively high pigment loading, in which the glass phase is relatively diluted. Accordingly, the decrease in the amount of binding glass oxides (Pb and K) relative to DW-W was assumed to be due to local dilution of the glass phase by the pigment. These outcomes are commonly encountered in point EDS measurements of a phase-heterogeneous enamel system (Domoney et al., 2011).

In DW-0, a composition of 32.14 wt.% Si, 9.38 wt.% Al, 10.58 wt.% Pb, 6.02 wt.% K, 0.93 wt.% Na and 1.66 wt.% Fe was measured and was interpreted as consistent with a glass matrix formulated on an Al-rich aluminosilicate (feldspathic) framework and adjusted with a moderate Pb-alkali flux. In overglaze enamel technologies, such 'framework-dominant, flux-adjusted' glass recipes are widely reported (Colomban et al. 2018; Colomban, 2022a; Colomban et al., 2022b). The direct detection of Fe (~1.66 wt.%) was regarded as strong micro-evidence that the orange hue was produced by iron-oxide pigments dispersed in lead(-alkali) glass matrices, and it is well documented in historical overglaze enamels (Hashimoto, et al., 2016a; Hashimoto et al., 2016b). It is widely recognized that enamels have a heterogeneous microstructure comprising pigment grains and glassy binder. Accordingly, Fe signal intensities in single-point EDS are expected to vary with intra-field distribution. Nevertheless, the detection of Fe in DW-0 was considered to indicate the presence of pigment grains at the analyzed spot (Beltrán et al., 2020).

The EDS point results were broadly consistent with the principal trends observed by XRF:

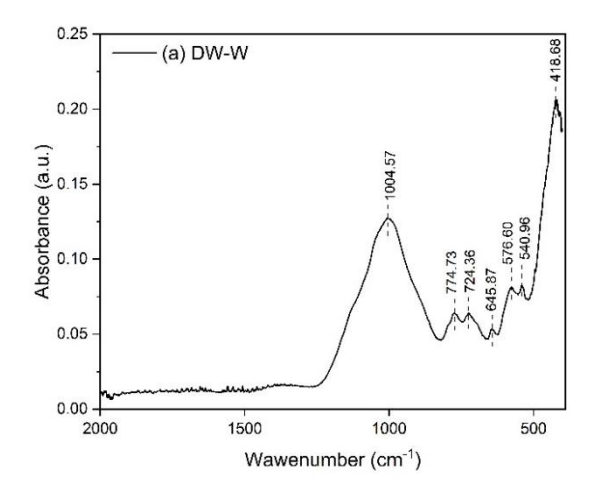
- (i) The ordering of Pb abundance (DW-W>DW-B>DW-O) was found to be the same by both methods. It was considered to indicate a more dominant lead-bearing glass binder in DW-W.
- (ii) The Al/Si ratio was the highest in DW-0, which was consistent with the highest Al_2O_3 content of DW-0 in XRF.

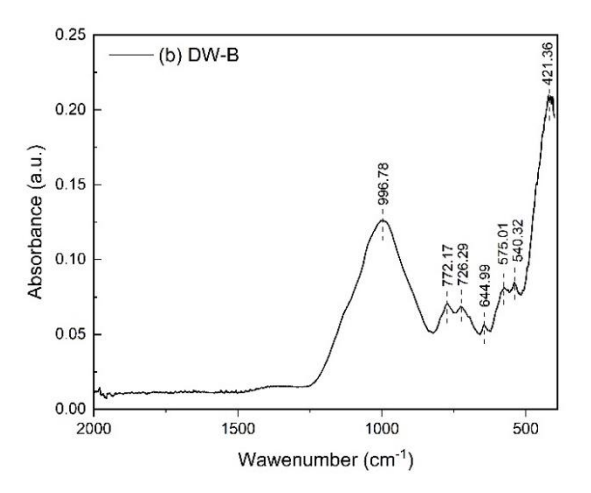
With respect to potassium (K), XRF was found to indicate comparatively higher K_2O in DW-B, whereas the local K measured by EDS was lower. This difference was attributed to the prominent C signal in the black enamel (~ 13 wt.%). This signal was assumed to locally dilute the glass phase, thereby causing K and Pb to be reported as lower. When this methodological difference was considered, no logical inconsistency was identified between EDS and XRF; rather, EDS was regarded as complementing the mass-averaged composition from

XRF with microscale evidence.

3.3. FT-IR Analysis

The degree of polymerization of the silicate glass network, the ring, bending, and stretching modes, and the potential effects of network modifiers in the examined enamels were investigated by FT-IR. The FT-IR spectra of DW-W, DW-B, and DW-O are presented in Figure 2.





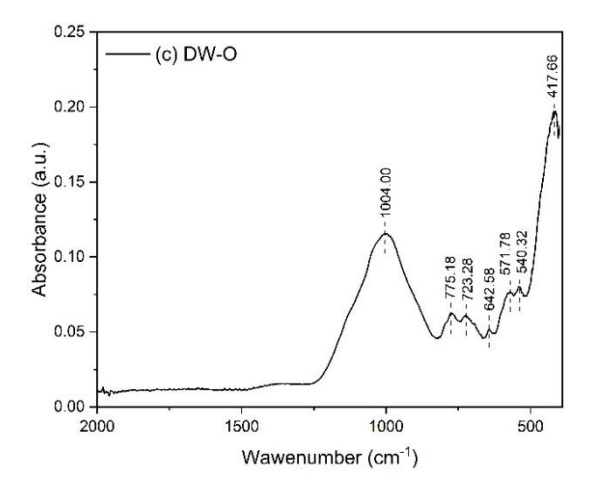


Figure 2. FT-IR spectra of (a) DW-W, (b) DW-B, and (c) DW-O.

As it is evident from Figure 2, the FT-IR spectra of the three moriage enamels exhibit shared band architecture indicative of a common silicate-glass framework. In DW-W, a band at 418.68 cm⁻¹ was observed and was assigned to the Si-O-Si bending (rocking) mode. In vitreous silica and silicate glass, a strong low-frequency bending band near 430 cm-1 is considered a fingerprint. Slight redshifts toward ~419 cm⁻¹ are expected in the presence of network-modifying cations (e.g., Pb, K, Na), which are known to alter bond angles and force constants (McMillan, 1984; Taylor, 1990). Similar bands at 421.36 cm-1 in DW-B and 417.66 cm-1 in DW-O were likewise assigned to the Si-O-Si bending mode, and the observed red shifts were considered consistent with modification of the silicate network by heavy/alkali cations. Furthermore, the prominence of bands around 418-421 cm⁻¹ in all three colors was considered to indicate the predominance of an amorphous silicate network at low frequencies rather than crystalline quartz (McMillan, 1984).

For all examined enamel, a band near ~540 cm⁻¹ (DW-W: 540.96, DW-B: 540.32, and DW-O: 540.32 cm-1) was observed and assigned to a composite of Al-O-Si and Si-0-(M) bending submodes, where M is alkali/heavy cation (including Si-O-(Pb/K/Na)). In aluminosilicate glass, a band near ~560 cm⁻¹ is assigned to Al-O-Si bridge, while the 530-580 cm⁻¹ band group is attributed to Si-O-(M)) bending subcomponents. Accordingly, the peak at ~541 cm-1 is consistent with contributions from both (Poggetto et al., 2021). Fine splitting in the bending region is known to be sensitive to Al incorporation and to the amount of network modifiers. Al-rich bridging is expected to shift band slightly upward, whereas network depolymerization shifts it slightly downward (Taylor, 1990). Therefore, the ~540 cm⁻¹ band observed in all three colors was considered consistent with Al-bearing bridges together with bending components enhanced in the presence of network modifiers (Li et al., 2023).

Bands at $\sim 571-576$ cm⁻¹ -576.60 in DW-W, 575.01 in DW-B, and 571.78 cm⁻¹ in DW-O- were observed and were attributed to AL-O-Si bridges and ring-like submodes. In aluminosilicate glasses, features in the 570-590 cm⁻¹ region are assigned to these modes and are regarded as the higher-frequency component relative to the Al-O-Si band near ~560 cm⁻¹ (Li et al., 2023). In studies on silicate glasses. The 500-700 cm⁻¹ band group is reported to comprise ring vibrations and bending modes. The intensities and positions of these bands are described as composition dependent (Sitarz, 2011). Accordingly, the ~576 cm⁻¹ band was considered a bending submode strengthened by contributions from Al-bearing bridges and medium-range ring units (Sitarz, 2011; Li et al., 2023). Additionally, the relatively redshifted positions DW-B (575.01 cm-1) and DW-0 (571.78 cm-1) were considered to imply slight differences in Al-O-Si contributions/ ring statistics or local network modifier loading, and were taken to indicate a more relaxed submode (Taylor, 1990).

Similarly, in aluminosilicate glasses, the 640-650 cm⁻¹ band is reported to comprise contributions from the Al-O-Si symmetric stretching and ring modes. In amorphous silica, the same interval is recognized as the upper end of the 500-700 cm⁻¹ band group to which ring-type Si-O-Si contribute (Sitarz, 2011; Li et al., 2023). In all enamels (645.87 in DW-W, 644.99 in DW-B, and 642.58 cm⁻¹ in DW-O), this band was observed, and its presence was regarded as the expected signature of an amorphous glass matrix (McMillan, 1984).

In the FT-IR spectra of enamels, the 700-800 cm⁻¹ region is known to host Si-O-Si symmetric stretching vibrations, which provide key information on the silicate network. The bands detected in this region- 774.73 cm⁻¹ for DW-W, 772.17 cm⁻¹ for DW-B, and 775.18 cm⁻¹ for DW-Owere assigned to the Si-O-Si symmetric stretching band located at ~770-800 cm⁻¹ in vitreous silica and many glasses (McMillan, 1984). When the band positions were compared, the peak in DW-0 was observed at a higher wavenumber than the other colors. This finding was considered to indicate that the symmetric band in DW-0 was less red-shifted and its network was comparatively more polymerized. The slight blue shift was further believed to signify, relative to DW-B, a tendency toward a higher fraction of bridging oxygen (BO) and a lower fraction of non-bridging oxygen (NBO) (Taylor, 1990). Additionally, a lower-frequency secondary band at ~723-726 cm⁻¹ was observed in the spectrum of enamels. The 700-750 cm⁻¹ interval is reported to include ring vibrations in amorphous silica and the component of the Si-O-Si symmetric stretch that is shifted to lower wavenumbers under the influence of network-modifying cations in the glass network (Innocenzi, 2003). In vitreous silica, the symmetric Si-O-Si component is characterized by a weak band near ~800 cm⁻¹. As the network modifiers increase, this band is expected to broaden and shift to lower wavenumbers. Accordingly, the comparatively low positions at 724.36 cm⁻¹ in DW-W, $726.29~\text{cm}^{\text{-}1}$ in DW-B, and $723.28~\text{cm}^{\text{-}1}$ in DW-O are regarded as indicators of glass formation and the degree of network modification. The broad profiles in this region, in contrast to the narrow, sharp lines of crystalline quartz (~779-805 cm⁻¹), are accepted as evidence additional strongly supporting amorphous/glassy nature of the materials (Taylor, 1990; Innocenzi, 2003).

In silicate glasses, the asymmetric Si-O stretching band envelope in the $\sim\!900\text{-}1100~\text{cm}^{-1}$ region is recognized as a principal spectral domain and it is widely used as an indicator of network polymerization and, by extension, of the presence of non-bridging oxygen (NBO) (Liu et al., 2021). In FT-IR spectra of silicate glasses, bands and shoulders are typically observed within $\sim\!950\text{-}1100~\text{cm}^{-1}$ as a function of the Qn species distribution; the Q2 ($\sim\!970\text{-}980~\text{cm}^{-1}$) and Q3 ($\sim\!1080\text{-}1090~\text{cm}^{-1}$) components are taken to reflect the degree of network polymerization (Liu et al., 2020). As the fraction of NBO increases, red shifts from $\sim\!1100~\text{cm}^{-1}$ toward $\sim\!1000~\text{cm}^{-1}$ and

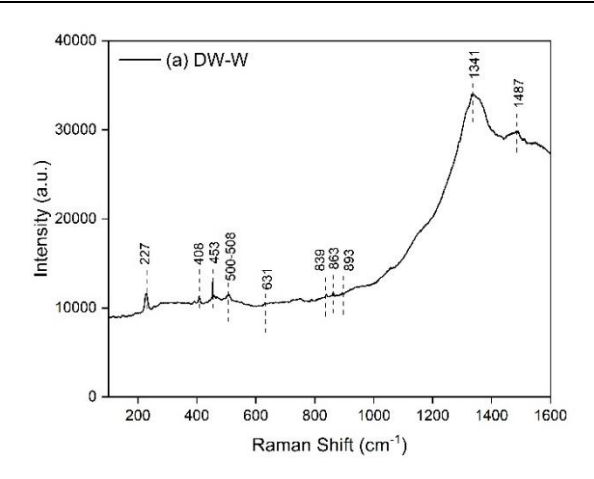
associated band broadening are observed (Taylor, 1990; Dalby and King, 2006). In DW-W and DW-O, a dominant band centered at 1004.57 and 1004 cm⁻¹, respectively, was observed, and these positions and profiles were considered consistent with a depolymerized (NBO-rich) aluminosilicate glass network. Shifts and broadenings into this region are frequently reported for Pb-alkali modified glasses (Serra et al., 2003; Liu et al., 2021). In DW-B, a band centered at ~996.8 cm⁻¹ was observed, lying at a lower wavenumber than DW-W and DW-O. This position was considered indicative of a more depolymerized glass network or higher network modifier loading (Dalby and King, 2006). In PbO-SiO2 glasses, the principal asymmetric Si-O stretching envelope is reported to shift with composition across ~960-1050 cm⁻¹ ¹, in correlation with decreasing network polymerization (Mihailova et al., 2023). Accordingly, a higher NBO/T ratio and, likely, more substantial Pb/K modification were inferred for DW-B.

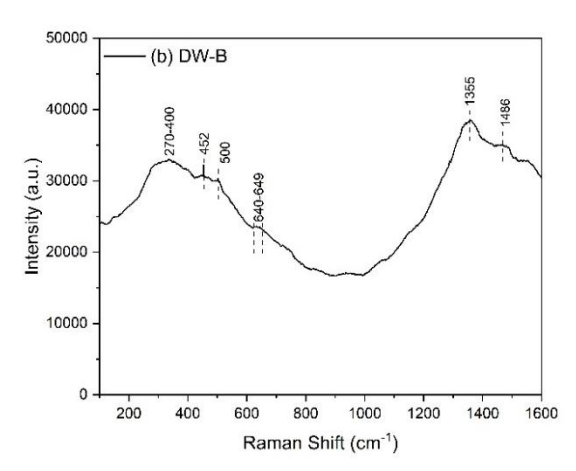
In summary, FT-IR is used to probe the Si/Al-O glass network in the mid-IR window, whereas Pb-O lattice modes are typically observed at lower (far-IR) frequencies. Accordingly, in this work, Pb was monitored indirectly, via the associated increase in depolymerization/non-bridging oxygen (De Sousa Meneses et al., 2006).

3.4. Raman Analysis

Within the scope of this study, Raman spectroscopy was employed to identify the specific pigment phases responsible for coloration in the differently colored moriage enamels and to elucidate the molecular structure of each sample. The Raman spectra for DW-W, DW-B, and DW-O are presented in Figure 3.

In DW-W, a weak mode around ~227 cm-1 was observed in the Raman spectrum and was assigned to a lowfrequency lattice/ring submode of the glass network. Nonetheless, no distinct crystalline phase was evidenced (McMillan, 1984). The 408-453 cm⁻¹ interval was attributed to subcomponents of the Si-O-Si band envelope, as expected for silicate glasses, which are known to broaden and redshift in the presence of leadalkali network modifiers (Colomban et al., 2006). The peak near 500-508 cm⁻¹ was considered consistent with the D1 breathing mode of four-membered rings in vitreous silica (~495 cm-1), whereas the broad component around ~631 cm-1 was regarded as consistent with the D2 mode of three-membered rings (~606 cm⁻¹), and both bands indicated the presence of a glassy phase (Gerbig and Michaels, 2020). In DW-W, weak peaks in the ~839-893 cm-1 region were observed and were assigned to sub-bands of the Si-O-Si symmetric stretch with contributions from small/medium ring units. These features were considered to represent the low-wavenumber flank of the glassy-silicate band envelope approaching ~900 cm⁻¹ (Colomban et al., 2006).





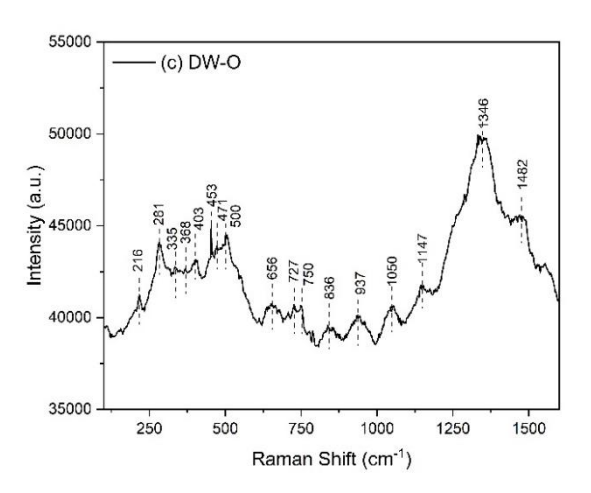


Figure 3. Raman spectra of (a) DW-W, (b) DW-B, and (c) DW-O.

The broad base around $\sim 1341~\rm cm^{-1}$ and $\sim 1487~\rm cm^{-1}$ was considered consistent with the low-wavenumber wing of the amorphous carbon D ($\sim 1350~\rm cm^{-1}$) and G ($\sim 1580~\rm cm^{-1}$) envelopes, respectively. Although carbon was not detected by EDS in DW-W, this was not considered contradictory, as the signal intensity in this region is often enhanced by aged organic binders (Ferrari and Robertson, 2000; Sadezky et al., 2005). Accordingly, the D/G like broadening in DW-W was regarded as compatible with trace, heterogeneously distributed carbonaceous matter rather than a bulk carbon phase.

In DW-B, a broad band spanning $\sim\!270\text{-}400~\text{cm}^{-1}$ was

observed and was attributed to the low-wavenumber wing of the Si-O-Si bending envelope, whereas the peak at ~452 cm⁻¹ was taken to reflect broadening of the Si-O-Si bending band under Pb/K modification (Colomban et al., 2006). As in DW-W, the feature near ~500 cm⁻¹ was considered consistent with the D1 breathing mode of four-membered rings, and the component in the ~600-649 cm⁻¹ range was regarded as the D2 counterpart arising from three-membered rings (Gerbig and Michaels, 2020). Broad bands at ~1355 cm⁻¹ and 1486 cm-1 were observed and were consistent with the D and G bands of amorphous carbon, supporting contributions from carbon black and soot, which is responsible for the black coloration (Ferrari and Robertson, 2000). Taken together with the FT-IR indicators of a more depolymerized glass (increased NBO/T), the Raman profile of DW-B was found to indicate a matrix dominated by amorphous glass and carbon additive (McMillan, 1984).

In DW-0, bands at ~221-225, ~281-293, and ~403-412 cm-1 were observed and were regarded as characteristic bands of hematite (α-Fe₂O₃). Additional modes near ~498-503 and ~613-660 cm⁻¹ were likewise consistent with this phase assignment. This attribution was further supported by the orange coloration and by the presence of Fe detected by EDS and XRF analysis (de Faria et al., 1997; Sparavigna, 2023). Consistent with the other colors, modes in the ~453-500 cm-1 interval were attributed to the Si-O-Si bending band and the D1 ring breathing component. Thereby confirming that the orange enamel was bound within an amorphous glaze/enamel-like matrix (McMillan, 1984; Gerbig and Michaels, 2020). Also in DW-0, broad bands near ~736 and 836 cm⁻¹ were observed and were assigned to lowerwavenumber submodes of the Si-O-Si symmetricstretching envelope arising from network-modifier effects (McMillan, 1984). Sub-bands at ~937, ~1050, and ~1147 cm-1 were evaluated as Q1-Q2 weighted Si-O stretching components characteristic of depolymerized Pb-alkali modified silicate glasses (Bengtsson et al., 2022). Bands around ~1346 and ~1482 cm⁻¹ were considered consistent with contributions from the amorphous carbon D/G envelopes (Ferrari and Robertson, 2000). Overall, the Raman profile of DW-0, including its Fe-oxide signatures, was found to be consistent with the XRF and EDS analysis. At the same time, the 900-1200 cm⁻¹ sub-bands corroborated the presence of a Pb-modified/aluminosilicate glass matrix, in parallel with the Si-O asymmetric-stretching envelope observed by FT-IR (de Faria, et al., 1997; Colomban et al., 2006).

Overall, the Raman spectra obtained in this study exhibited broad glass bands in the 430-900 and 900-1200 cm⁻¹ regions, together with the D1 and D2 ring modes. This was taken to indicate that an amorphous Pbalkali silicate matrix predominated at the surfaces of the examined materials (McMillan, 1984; Gerbig and Michaels, 2020). The quartz fingerprint peak at 464-465

cm⁻¹ and its associated low-frequency lines were not observed. Instead, the bands around 450-520 cm⁻¹ behaved as the glassy D1 and the Si-O-Si bending envelope rather than sharp crystalline lines (Ostroumov et al., 2002).

4. Conclusions

In this study, a multi-technique analytical framework was adopted to elucidate the material architecture of the moriage enamels on a Japanese Dragonware plate. A bulk-scale chemical framework was established by XRF, and micrometer-scale contextual information was added by SEM-EDS. Owing to the phase-selective and network-sensitive character of FT-IR and Raman spectroscopy, technological inferences beyond composition were enabled.

Color-based findings suggested that the layer formulations were functionally optimized. In DW-W (white), the relatively high contents of Pb and alkali oxides were found to be consistent with a low-melting, highly fluid Pb-alkali silicate binder. In DW-B (black), the pronounced carbon contribution, together with comparatively lower K/Si and Pb/Si ratios, was attributed to local dilution of the glass phase by the pigment loading. The D/G band morphology in the Raman spectra of DW-B was considered to indicate the use of carbon black or soot in the black coloration. In DW-0 (orange), an Al-rich feldspathic framework together with hematite $(\alpha-Fe_2O_3)$ signatures was identified, and the layer was considered consistent with the dispersion of Fe-oxide pigment within a feldspathic glass matrix. Differences in peak positions and bandwidth within the Si-O-Si symmetric and asymmetric stretching modes were observed, indicating that the degree of network polymerization varied among the colors. Technologically, the findings were entirely consistent with the overglaze character of the moriage application. The FT-IR signatures of a strongly Pb-alkalimodified glass network were found to be consistent with the requirements of a low melting/viscosity threshold and low temperature flow.

Based on these results, conservation and museum practices for multilayer overglaze decorations such as moriage are required to be conducted under preventive conservation principles centered on the production technology. Accordingly, to mitigate the risks of alkali loss (alkali leaching) and Pb-ion leaching, display and storage environments are recommended to target 50 ± 5% relative humidity and 18-22 °C, and sources of volatile organic acids (e.g., acetic/formic acid) are to be excluded. Owing to the potential for smearing and staining associated with carbon black/soot confirmed by Raman spectroscopy in the black areas, surface interventions are to be limited to dry and minimally invasive methods (soft brushing, micro-aspiration, powder-free nitrile gloves); where wet cleaning is unavoidable, a spot test should be performed first and neutral-pH, deionized (DI) water with non-abrasive, nonchelating swabs should be employed. In the cleaning of multilayer overglaze decorations such as moriage, the use of alkaline detergents, strong solvents such as ethanol/acetone, and excessive mechanical rubbing is strongly discouraged. In addition, in view of the susceptibility of enamel crack networks to capillary water transport, moisture fluctuations should be prevented, and light levels should be kept low. Signs of alkali leaching (e.g., matting, iridescence) should be monitored through routine visual checklists; where treatment/retouching required, reversible. is conservation-grade resins should be preferred, and fill/inpainting materials should be pre-tested for glassceramic compatibility and for thermal/surface expansion behavior.

Author Contributions

The percentages of the author' contributions are presented below. The author reviewed and approved the final version of the manuscript.

	D.T.B
С	100
D	100
S	100
DCP	100
DAI	100
L	100
W	100
CR	100
SR	30
PM	100
FA	100

C=Concept, D= design, S= supervision, DCP= data collection and/or processing, DAI= data analysis and/or interpretation, L= literature search, W= writing, CR= critical review, SR= submission and revision, PM= project management, FA= funding acquisition.

Conflict of Interest

No conflict of interest or common interest has been declared by the author.

Ethical Consideration

Ethics committee approval was not required for this study because of there was no study on animals or humans.

Acknowledgements

The author sincerely thanks Prof. Dr. Ahmet KOLUMAN for the generous donation of the Dragonware plate from his collection for this study, and Dr. Ahmet ERDEM for his contributions to the FT-IR analyses.

References

- Anonymous. (2024). *Moriage technique*. International Nippon Collectors Club. Retrieved September 17, 2025, from https://nipponcollectorsclub.com/nippontechniques/moriage
- Anonymous. (2025). *Itchin-gaki*. Kogeistandard. Retrieved September 17, 2025, from https://www.kogeistandard.com/resource/itchin
- Bell, I. M., Clark, R. J., & Gibbs, P. J. (1997). Raman spectroscopic library of natural and synthetic pigments (pre-≈1850 AD). Spectrochimica Acta Part A: Molecular and Biomolecular Spectroscopy, 53(12), 2159–2179.
- Beltrán, M., Schibille, N., Brock, F., Gratuze, B., Vallcorba, O., & Pradell, T. (2020). Modernist enamels: Composition, microstructure and stability. *Journal of the European Ceramic Society*, 40(4), 1753–1766.
- Bengtsson, F., Pehlivan, I. B., Österlund, L., & Karlsson, S. (2022). Alkali ion diffusion and structure of chemically strengthened TiO₂ doped soda-lime silicate glass. *Journal of Non-Crystalline Solids*. 586, 121564.
- Bezur, A., & Casadio, F. (2013). The analysis of porcelain using handheld and portable X-ray fluorescence spectrometers. In *Handheld XRF for art and archaeology* (pp. 249–312).
- Boon, J. J., & Asahina, S. (2006). Surface preparation of cross sections of traditional and modern paint using the Argon ion milling polishing CP system. *Microscopy and Microanalysis*, 12(S02), 1322–1323.
- Colomban, P. (2004). Raman spectrometry, a unique tool to analyze and classify ancient ceramics and glasses. *Applied Physics A*, 79(2), 167–170.
- Colomban, P. (2022a). Full spectral range Raman signatures related to changes in enameling technologies from the 18th to the 20th century: Guidelines, effectiveness and limitations of the Raman analysis. *Materials*, *15*(9), 3158.
- Colomban, P., Gallet, X., Simsek Franci, G., Fournery, N., & Quette, B. (2024). Non-invasive Raman classification comparison with pXRF of monochrome and related Qing porcelains: Lead-rich, lead-poor-, and alkali-based glazes. *Materials*, *17*(14), 3566.
- Colomban, P., Gironda, M., Simsek Franci, G., & d'Abrigeon, P. (2022). Distinguishing genuine Imperial Qing dynasty porcelain from ancient replicas by on-site non-invasive XRF and Raman spectroscopy. *Materials*, 15(16), 5747.
- Colomban, P., Maggetti, M., & d'Albis, A. (2018). Non-invasive Raman identification of crystalline and glassy phases in a 1781 Sèvres Royal Factory soft paste porcelain plate. *Journal of the European Ceramic Society, 38*(15), 5228–5233.
- Colomban, P., Ngo, A. T., & Fournery, N. (2022b). Non-invasive Raman analysis of 18th century Chinese export/armorial overglazed porcelain: Identification of the different enameling techniques. *Heritage*, *5*(1), 233–259.
- Colomban, P., Tournie, A., & Bellot-Gurlet, L. (2006). Raman identification of glassy silicates used in ceramics, glass and jewellery: A tentative differentiation guide. *Journal of Raman Spectroscopy*, *37*(8), 841–852.
- Coman, S. (2021). *Meiji period, an introduction*. Smarthistory. Retrieved November 19, 2025, from https://smarthistory.org/meiji-period/
- Dal Poggetto, G., D'Angelo, A., Blanco, I., Piccolella, S., Leonelli, C., & Catauro, M. (2021). FT-IR study, thermal analysis, and evaluation of the antibacterial activity of a MK-geopolymer mortar using glass waste as fine aggregate. *Polymers*, 13(17), 2970.
- Dalby, K. N., & King, P. L. (2006). A new approach to determine and quantify structural units in silicate glasses using micro-

- reflectance Fourier-transform infrared spectroscopy. *American Mineralogist*, *91*(11–12), 1783–1793.
- Davila, L. P., Risbud, S. H., & Shackelford, J. F. (2008). Quartz and silicas. In J. F. Shackelford & R. H. Doremus (Eds.), *Ceramic and glass materials: Structure, properties and processing* (pp. 78–79). Springer.
- de Faria, D. L. A., Venâncio Silva, S., & de Oliveira, M. T. (1997).

 Raman microspectroscopy of some iron oxides and oxyhydroxides. *Journal of Raman Spectroscopy*, 28(11), 873–878
- De Sousa Meneses, D., Malki, M., & Echegut, P. (2006). Structure and lattice dynamics of binary lead silicate glasses investigated by infrared spectroscopy. *Journal of Non-Crystalline Solids*, 352(8), 769–776.
- Domoney, K., Shortland, A. J., & Kuhn, S. (2011). Characterization of 18th-century Meissen porcelain using SEM-EDS. *Archaeometry*, *54*(3), 454-474.
- Ferrari, A. C., & Robertson, J. (2000). Interpretation of Raman spectra of disordered and amorphous carbon. *Physical Review B*, *61*(20), 14095.
- Gerbig, Y. B., & Michaels, C. A. (2020). In-situ Raman spectroscopic measurements of the deformation region in indented glasses. *Journal of Non-Crystalline Solids*, 530, 119828.
- Giannossa, L. C., Forleo, T., & Mangone, A. (2021). The distinctive role of chemical composition in archaeometry: The case of Apulian red figure pottery. *Applied Sciences*, 11(7), 3073.
- Hall, M. E. (2017). X-ray fluorescence-energy dispersive (ED-XRF) and wavelength dispersive (WD-XRF) spectrometry. In
 A. M. W. Hunt (Ed.), The Oxford handbook of archaeological ceramic analysis (p. 342). Oxford University Press.
- Hashimoto, H., Higuchi, K., Inada, H., Okazaki, Y., Takaishi, T., & Asoh, H. (2016a). Well-dispersed α-Fe₂O₃ particles for lead-free red overglaze enamels through hydrothermal treatment. *ACS Omega*, 1(1), 9–13.
- Hashimoto, H., Inada, H., Okazaki, Y., Takaishi, T., Fujii, T., Takada, J., & Asoh, H. (2016b). Controlling the color of lead-free red overglaze enamels and a process for preparing high-quality red paints. *ACS Applied Materials & Interfaces*, 8(17), 10918–10928.
- Hunt, A. M. W., & Speakman, R. J. (2015). Portable XRF analysis of archaeological sediments and ceramics. *Journal of Archaeological Science*, 53, 626–638.
- Inada, H., Okazaki, Y., Yokoyama, T., Takaishi, T., Fujii, T., Takada, J., Asoh, H., & Hashimoto, H. (2018). Interaction between lead-free multicomponent alkali borosilicate glass frits and hematite in red overglaze enamels. *Journal of the American Ceramic Society*, 101(10), 4538–4548.
- Innocenzi, P. (2003). Infrared spectroscopy of sol-gel-derived silica-based films: A spectra-microstructure overview. *Journal of Non-Crystalline Solids*, *316*, 309–319.
- Jiusti, J., Zanotto, E. D., Feller, S. A., Austin, H. J., Detar, H. M., Bishop, I., Manzani, D., Nakatsuka, Y., Watanabe, Y., & Inoue, H. (2020). Effect of network formers and modifiers on the crystallization resistance of oxide glasses. *Journal of Non-Crystalline Solids*, 550, 120359.
- Li, M., Dong, C., Ma, Y., & Jiang, H. (2023). Light-transmitting lithium aluminosilicate glass-ceramics with excellent mechanical properties based on cluster model design. *Nanomaterials*, *13*(3), 530.
- Li, Y., Liu, P., Luo, Y., Ge, M, Xing, H., & Li, Y. (2024). Corrosion mechanisms for lead-glazed pottery from Qibi Ming Tomb of the Tang Dynasty in Xianyang, China. *Heritage Science*, 12, 224.
- Liu, G. L., & Kazarian, S. G. (2022). Recent advances and applications to cultural heritage using ATR-FTIR spectroscopy

- and ATR-FTIR spectroscopic imaging. *Analyst, 147*(9), 1777–1797.
- Liu, H., Hahn, S. H., Ren, M., Thiruvillamalai, M., Gross, T. M., Du, J., van Duin, A. C. T., & Kim, S. H. (2020). Searching for correlations between vibrational spectral features and structural parameters of silicate glass network. *Journal of the American Ceramic Society*, 103(6), 3575–3589.
- Liu, H., Kaya, H., Lin, Y. T., Ogrinc, A., & Kim, S. H. (2021). Vibrational spectroscopy analysis of silica and silicate glass networks. *Journal of the American Ceramic Society*, 105(4), 2355–2384.
- McMillan, P. (1984). Structural studies of silicate glasses and melts—Applications and limitations of Raman spectroscopy. *American Mineralogist*, 69(7–8), 622–644.
- Mihailova, I., Harizanova, R., Tasheva, T., Dimova, N., & Rüssel, C. (2023). Physicochemical and structural characterization of silicate glasses containing iron oxides. *Journal of Chemical Technology and Metallurgy*, 58(1), 3–7.
- Mommsen, H., Beier, T., Diehl, U., & Podzuweit, C. (1992). Provenance determination of Mycenaean sherds found in Tell el Amarna by neutron activation analysis. *Journal of Archaeological Science*, 19(3), 295–302.
- Moropoulou, A., Zendri, E., Ortiz, P., Delegou, E. T., Ntoutsi, I., Balliana, E., Becerra, J., & Ortiz, R. (2019). Scanning microscopy techniques as an assessment tool of materials and interventions for the protection of built cultural heritage. *Scanning*, 2019, 5376214.
- Nilsson, J. E. (2023). *Dragonware*. Gotheborg. Retrieved September 17, 2025, from https://www.gotheborg.com/glossary/dragonware.shtml
- Nilsson, J. E. (2023). *Moriage (piling-up)*. Gotheborg. Retrieved September 17, 2025, from https://www.gotheborg.com/glossary/moriage.shtml
- Ostroumov, M., Faulques, E., & Lounejeva, E. (2002). Raman spectroscopy of natural silica in Chicxulub impactite, Mexico. *Comptes Rendus Geoscience*, 334(1), 21–26.
- Öz, C., & Özer, Ö. (2019). Seramik arkeometrisi'nde spektroskopik yöntemlerin uygulanması ve yorumlanması: XRF, XRD. Seramik Araştırmaları Dergisi, 1, 136–153.
- Papliaka, Z. E., Vaccari, L., Zanini, F., & Sotiropoulou, S. (2015). Improving FTIR imaging speciation of organic compound residues or their degradation products in wall painting samples using a new thin section preparation strategy based on cyclododecane pre-treatment. *Analytical and Bioanalytical Chemistry*, 407(18), 5393–5403.
- Perna, M. G., Falcone, F., Casolino, C., Metalla, E., Rosatelli, G., Antonelli, S., & Stoppa, F. (2024). Analysing the glaze of a medieval ceramic fragment from the Durres amphitheater in Albania. *Heritage Science*, 12, 82.
- Pięta, E., Olszewska-Świetlik, J., Paluszkiewicz, C., Zając, A., & Kwiatek, W. M. (2019). Application of ATR-FTIR mapping to identification and distribution of pigments, binders and degradation products in a 17th century painting. *Vibrational Spectroscopy*, 103, 102928.
- Pięta, E., Proniewicz, E., Szmelter-Fausek, B., Olszewska-Świetlik, J., & Proniewicz, L. M. (2014). Micro-Raman spectroscopy analysis of the 17th century panel painting "Servilius Appius" by Isaac van den Blocke. *Journal of Raman Spectroscopy*, 45(11–12), 1019–1025.
- Pradell, T., & Molera, J. (2020). Ceramic technology: How to characterise ceramic glazes. *Archaeological and Anthropological Sciences*, 12, 189.
- Prati, S., Joseph, E., Sciutto, G., & Mazzeo, R. (2010). New advances in the application of FTIR microscopy and

- spectroscopy for the characterization of artistic materials. *Accounts of Chemical Research*, 43(6), 792–801.
- Prati, S., Sciutto, G., Bonacini, I., & Mazzeo, R. (2016). New frontiers in application of FTIR microscopy for characterization of cultural heritage materials. *Topics in Current Chemistry*, 374, 26.
- Qu, L., Zhang, X., Duan, H., Zhang, R., Li, G., & Lei, Y. (2017). The application of LIBS and other techniques on Chinese low temperature glaze. MRS Advances, 2(39), 2081–2094.
- Ravindran, T., Arora, A. K., Ramya, S., Subba Rao, R., & Raj, B. (2011). Raman spectroscopic study of medieval Indian art of 17th century. *Journal of Raman Spectroscopy*, 42(4), 803–807.
- Ricci, G. (2016). Archaeometric studies of historical ceramic materials (Doctoral dissertation). Universita Ca' Foscari Venezia.
- Sadezky, A., Muckenhuber, H., Grothe, H., Niessner, R., & Pöschl, U. (2005). Raman microspectroscopy of soot and related carbonaceous materials: Spectral analysis and structural information. *Carbon*, 43(8), 1731–1742.
- Scimeca, M., Bischetti, S., Lamsira, H. K., Bonfiglio, R., & Bonanno, E. (2018). Energy dispersive X-ray (EDX) microanalysis: A powerful tool in biomedical research and diagnosis. *European Journal of Histochemistry*, *62*(1), 2841.
- Serra, J., González, P., Liste, S., Serra, C., Chiussi, S., León, B., Pérez-Amor, M., Ylänen, H. O., & Hupa, M. (2003). FTIR and XPS studies of bioactive silica based glasses. *Journal of Non-Crystalline Solids*, 332, 20–27.
- Sitarz, M. (2011). The structure of simple silicate glasses in the light of middle infrared spectroscopy studies. *Journal of Non-Crystalline Solids*, *357*(6), 603–608.
- Smith, G. D., & Clark, R. J. H. (2004). Raman microscopy in archaeological science. *Journal of Archaeological Science*, 31(8), 1137–1160.
- Sparavigna, A. C. (2023). Raman spectroscopy of the iron oxides in the form of minerals, particles and nanoparticles. *ChemRxiv*. Retrieved September 24, 2025, from http://www.edpsciences.org/docinfos/INRARND
- Szökefalvi-Nagy, Z., Demeter, I., Kocsonya, A., & Kovács, I. (2004). Non-destructive XRF analysis of paintings. Nuclear Instruments and Methods in Physics Research Section B, 226, 53–59.
- Taylor, W. (1990). Application of infrared spectroscopy to studies of silicate glass structure: Examples from the melilite glasses and the systems Na₂O-SiO₂ and Na₂O-Al₂O₃-SiO₂. *Proceedings of the Indian Academy of Sciences, 99*(1), 99–117.
- Tite, M. S., Freestone, I., Mason, R., Molera, J., Vendrell-Saz, M., & Wood, N. (1998). Lead glazes in antiquity—Methods of production and reasons for use. *Archaeometry*, 40(2), 241–260.
- Turco, F., Davit, P., Cossio, R., Agostino, A., & Operti, L. (2017).
 Accuracy improvement by means of porosity assessment and standards optimization in SEM-EDS and XRF elemental analyses on archaeological and historical pottery and porcelain. *Journal of Archaeological Science: Reports, 12*, 54–65.
- Veeramuthu, K., Sekar, S. C., & Saravanan, D. (2014). Characteristic analysis of archaeological pottery recently excavated from the site Mayiladumparai, Krishnagiri District, Tamil Nadu, India by analytical techniques. *International Journal of Chemical Studies*, 2(1), 64–68.
- Weber, J., Beier, T., Diehl, U., Lambrecht, D., Mommsen, H., & Pantenburg, F. (1990). A PIXE mini-beam setup at the Bonn cyclotron for archeometric metal analyses. *Nuclear Instruments and Methods in Physics Research Section B*, 50(1–4), 221–225.

Willman, A. (2011). Edo-period Japanese porcelain. Heilbrunn Timeline of Art History. The Metropolitan Museum of Art. Retrieved November 19, 2025, from https://www.metmuseum.org/essays/edo-period-japanese-porcelain

Wu, J., & Stebbins, J. F. (2009). Effects of cation field strength on the structure of aluminoborosilicate glasses: High-resolution 11B, 27Al and 23Na MAS NMR. *Journal of Non-Crystalline Solids*, 355(9), 556–562.